The role of continental lithospheric thermal structure in the evolution of orogenic systems: Application to the Himalayan-Tibetan collision zone

Mengxue Liu[1], Dinghui Yang[1], Rui Qi[1]

[1]Department of Mathematical Sciences, Tsinghua University, Beijing 100084, China.

Correspondence to: Dinghui Yang (ydh@mail.tsinghua.edu.cn)

Abstract. Continental collision is a crucial process in plate tectonics. However, in terms of the evolution and the controlling parameters of its lateral heterogeneity, our understanding of the tectonic complexities at such a convergent plate boundary remains largely unclear. In this study, we conducted a series of two-dimensional numerical experiments to investigate how continental lithospheric thermal structure influences the development of lateral heterogeneity along the continental collision zone. Two end members were achieved: 1) Continuous subduction mode, which prevails when the model has a cold procontinental moho temperature ($\leq$ 450 ˚C). In this case, a narrow collision orogen develops, and the subducting angle steepens with the increasing retrocontinental moho temperature. 2) Continental subduction with a slab break-off, which generates a relative wide collision orogen, and dominates when the model has a relatively hot procontinental moho temperature ($\geq$ 500 ˚C), especially when the moho temperature $\geq$ 550˚C. Radioactive heat production is the second-order controlling parameter in varying the continental collision mode, while it prefers to enhance strain localization in the upper part of the continental lithosphere and promote the growth of shear zones there. By comparing the model results with geological observations, we suggest that the discrepant evolutionary paths from the continuous subduction underlying the Hindu Kush to the continental subduction after slab break-off beneath eastern Tibet may originate from the inherited lateral inhomogeneity of Indian lithospheric thermal structure. Besides, the high content of crustal radioactive elements may be one of the most important factors that controls the formation of large thrust fault zones in the Himalayas.

1 Introduction

The collision between the Indian and Asian continents following the closure of the Neo-Tethys Ocean is regarded as one of the key geodynamical processes of plate tectonics (Toussaint et al., 2004), which creates the world's largest orogen (the Alpine-Himalaya orogen) and highest plateau (the Tibetan Plateau). It would be really hard to maintain a homogeneous plate morphology and the crustal-mantle deformation features during such a large-scale collision stretching thousands of kilometers. Many of the previous observations have already provided insights into the significant lateral heterogeneity of Himalayan-Tibetan orogen (Zhou and Murphy, 2005; Li et al., 2008; Chen et al., 2015). Specifically, the horizontal underthrusting distance of the Indian lithosphere decreases and the subducting angle increases laterally from west to east.

1

Despite various mechanisms have been invoked, including geometry of the subducting plate (Nettesheim et al., 2018; Koptev et al., 2019), inhomogeneous inherit lithospheric structure, variations in rock composition, characters of terrane assembly, and the complex tectonic settings (Beaumont et al., 2004; Chen et al., 2016, 2019; Vogt et al., 2018; Liu and Yang, 2022), the development of the collision zone's lateral heterogeneity remains ambiguous and requires further investigations.

Many of the laboratory experiments (Willingshofer and Sokoutis, 2009; Luth et al., 2010) and numerical modeling (Beaumont et al., 1994; Pysklywec, 2001; Toussaint et al., 2004; Huangfu et al., 2017; Liao and Gerya, 2017; Vogt et al., 2018; Liu et al., 2022b) have suggested that lithospheric thermal structure is one of the important controlling parameters contributing to the regulation the evolution of continental collision (Pysklywec, 2001; Faccenda et al., 2008; Ueda et al., 2012; Tang et al., 2020; Liu et al., 2022a). Pysklywec (2001) once used a series of thermomechanical models that focused on the evolutionary modes of the continental lithospheric mantle during collision. The experiments suggested that an increase in lithospheric geotherm resulted in a transition of the lithospheric mantle from an asymmetric, subduction-like mode to ablative subduction. Similarly, on the basis of two-dimensional mechanical models, Toussaint et al. (2004) investigated the potential scenarios for the evolution of continental collision. They concluded that models with a relatively low (< 550 ˚C) moho temperature and a fast convergent rate (> 5 cm/yr) are more likely to maintain stable subduction. On the contrary, among warmer and slower convergent models, lithospheric folding, pure-shear thickening, and Rayleigh-Taylor (RT) instabilities prevailed. Ghazian and Buiter (2013) used 2D numerical models to discuss the sensitivity of various collision modes to velocity, crust-mantle temperature structure, lithospheric rheology, and the density difference between the lithospheric mantle and asthenosphere. They recognized that velocity, lithospheric rheology, and temperature have important controls. More precisely, stable continental subduction evolves over a large range of values for convergent velocity and lithospheric temperature. Fast and cold models tend to fold, while slow and warm ones can generate RT-type dripping. Heron and Pysklywec (2016) subsequently presented dynamic thermomechanical experiments to explore the role of lithospheric inherited weakness in the orogenic process. According to their model results, lithospheric temperature exerts a strong control on lithospheric strength; it may influence the brittle-ductile transition depth to help determine which layer (upper crust, lower crust, or lithospheric mantle) dominantly controls the lithospheric deformation style in a collision system. Recently, Huangfu et al. (2019) employed systematic numerical simulations to study the dynamics of the lithospheric-scale subduction and crustal-scale underthrusting of the continental collision zone. They found that models with low convergence velocity and a cold upper plate are inclined to lithospheric-scale subduction, whereas models with high velocity and a hot overriding plate contribute to crustal-scale underthrusting. Though numerous numerical simulations are employed to qualify the effects of lithospheric thermal structure, it is noteworthy, however, that earlier studies consistently mainly focused on the influences of the overriding lithospheric thermal structure. A fairly large number of them neglected oceanic subduction prior to the continental collision for simplicity. Thus, our understanding of tectonic complexities that may emerge during progressive crust-mantle deformation at the convergent plate boundary remains largely unclear.

Here we present a series of high-resolution numerical experiments to gain new insights on how continental lithospheric thermal structure influences the evolutionary path of the continental collision system. Temperature

64 heterogeneities are incorporated by altering the continental moho temperature (T_{moho}) and crustal radioactive heat production

65 (H_r), respectively. In the end, the results of our models are used to draw comparisons with some first-order characters of the

66 Indian-Asian collision zone.

2 Materials and Methods

2.1 Governing equation

69 We use the parallel code **A**dvanced **S**olver for **P**roblems in **E**arth's **C**onvec**T**ion (ASPECT) (Kronbichler et al., 2012),

70 an extensible code of the C++ program library deal.ii (**D**ifferential **E**quations **A**nalysis **L**ibrary, https://www.dealii.org/),

71 targeted at the computational solution of partial differential equations using adaptive finite elements (Arndt et al., 2021), to

72 solve three conservation equations. The methodology is similar to our recent work (Liu and Yang, 2022; Liu et al., 2022a).

73 The models are calculated by solving the following equations of conservation of mass, momentum, and internal energy for

74 an incompressible medium and adopting the extended Boussinesq approximation (van Zelst, 2022).

$$-\nabla \cdot 2\eta\dot{\varepsilon}(\boldsymbol{u}) + \nabla p = \rho\mathbf{g} \qquad \text{in } \Omega, \tag{1}$$

$$\nabla \cdot \boldsymbol{u} = 0 \qquad \text{in } \Omega, \tag{2}$$

$$\rho_0 C_p \left(\frac{\partial T}{\partial t} + \boldsymbol{u} \cdot \nabla T \right) - \nabla \cdot k\nabla T = \rho_0 H \tag{3}$$

$$+ 2\eta\, \dot{\varepsilon}(\boldsymbol{u}) : \dot{\varepsilon}(\boldsymbol{u})$$

$$+ \alpha T (\boldsymbol{u} \cdot \nabla P) \qquad \text{in } \Omega$$

$$\frac{\partial c_i}{\partial t} + \boldsymbol{u} \cdot \nabla c_i = 0 \tag{4}$$

81 On the right hand-side of Eq. (3), the three terms represent the internal heat production that includes radioactive decay,

82 frictional heating, and adiabatic compression of material. η is the viscosity, $\dot{\varepsilon}(\boldsymbol{u}) = \frac{1}{2}(\nabla\boldsymbol{u} + \nabla\boldsymbol{u}^T)$ is the deviator of the

83 strain rate tensor, $\boldsymbol{u}$ is the velocity, p is the pressure, $\mathbf{g}$ is the gravitational acceleration, Ω is the interesting domain, C_p is the

84 heat capacity, k is the heat conductivity, H is the intrinsic specific heat production, α is the thermal expansion coefficient, ρ_0

85 is the adiabatic reference density. c_i named compositional fields here (e.g., upper crust, lower crust, Kronbichler et al., 2012).

86 As the medium was considered incompressible, we assumed that the density (ρ) in Eq. (1) satisfied the equation:

$$\rho = \rho_0 (1 - \alpha (T - T_0)) \tag{5}$$

88 where ρ_0 is the reference density at reference temperature T_0 (293 K).

3

2.2 Rheology

Our models are based on the common assumption that solid earth materials are treated as highly viscous fluids. Thus, we apply a viscoplastic rheology (Glerum et al., 2018). The viscous regime uses a composite of diffusion and dislocation creep that can be conveniently formulated as follows: (Karato and Wu, 1993; Karato, 2008).

$$\eta_{\text{diff/disl}} = \frac{1}{2} A_{diff/disl}^{-\frac{1}{n}} \, d^{\frac{m}{n}} \, \dot{\varepsilon}_e^{\frac{1-n}{n}} \exp\left(\frac{Q_{diff/disl} + PV_{diss/disl}}{nRT}\right) \tag{6}$$

$$\eta_{\text{comp}} = \left(\frac{1}{\eta_{\text{diff}}} + \frac{1}{\eta_{\text{disl}}}\right)^{-1} \tag{7}$$

where $\dot{\varepsilon}_e$ is the square root of second invariant of the deviatoric strain rate. In the case of diffusion creep, $n = 1$, $m > 0$, while for dislocation creep $n > 1$, $m = 0$. Definitions and values of other symbols are shown in Table S1 in Supporting Information. Surface erosion and sedimentation are neglected.

The plastic yielding is defined by the Drucker–Prager criterion as Eq. (8) (Davis and Selvadurai, 2002):

$$\eta_{\text{yield}} = \frac{C\cos(\phi) + P\sin(\phi)}{2\dot{\varepsilon}_e} \tag{8}$$

Where C is the cohesion and ϕ is the initial friction angle. We also include strain weakening in the plastic regime, through which C and ϕ are linearly weakened by a factor of 2 or 4 between plastic strains of 0.5 and 1.5.

The effective viscosity is eventually given by:

$$\eta_{\text{eff}} = \min\left(\max\left(\eta_{\text{i}}, \eta_{\text{min}}\right), \eta_{\text{max}}\right) \tag{9}$$

where i is one of the subscripts among diff, disl, comp, and yield. η_{max} and η_{min} are user-defined viscosity cutoffs (Table S1).

2.3 Initial model configuration and boundary conditions

The numerical model domain is 2000 km × 660 km in the horizontal and vertical directions. It contains a retrocontinental lithosphere and a procontinental lithosphere, with an oceanic lithosphere in between (Fig. 1). A weak zone with a width of 10 km (gabbro, Wilks and Carter, 1990) abuts the oceanic plate to facilitate subduction. The continental lithosphere is 120 km thick, consisting of a 25-km-thick upper crust (wet quartzite, Gleason and Tullis, 1995), a 10-km lower crust (wet anorthite, Rybacki et al., 2006), and an 85-km lithospheric mantle. The oceanic lithosphere (~ 90 Ma) contains a 4-km-thick sediment layer (gabbro, Wilks and Carter, 1990), an 8-km-thick oceanic crust layer (gabbro, Wilks and Carter, 1990), and an 88-km-thick lithospheric mantle. Dry olivine (Hirth and Kohlstedt, 2003) is used for the mantle. All material properties are listed in Table S1. The numerical resolution incrementally increases along the depth direction from 2 km × 2 km to 8 km × 8 km.

Temperature is fixed at the model surface (0˚C) and the base of the lithosphere (1300˚C), while various continental T_{moho} is defined ranging from 450 – 600 ˚C. The initial continental lithospheric temperature profile follows Chapman (1986), taking into account the thickness of each lithologic layer (Eqs. (11) - (13)). According to these equations, T_{moho} and Hr are

4

118 not independent parameters, we thus fixed T_{moho} when investigating the influence of H_r. Specially, we first choose a surface

119 (T_T), moho temperature (T_B), and radioactive heat production (H), then calculate the surface heat flow (q_T) based on Eq. (12).

120 After that, we substitute the above T_T, q_T, and H into Eq. (11) to get the continental crustal temperature structure. The

121 oceanic lithospheric temperature distribution follows the half-space cooling model (Turcotte and Schubert, 2002), and in all

122 models we use the same initial oceanic lithospheric thermal structure. Besides, a temperature gradient of 0.5 ˚C/km is

123 assumed for the sublithospheric mantle (Huangfu et al., 2019).

$$T_Z = T_T - \frac{q_T}{k}Z - \frac{H\,Z^2}{2k} \tag{11}$$

$$T_B = T_T + \frac{q_T}{k}\Delta Z - \frac{H\,\Delta Z^2}{2k} \tag{12}$$

$$q_B = q_T - H\Delta Z \tag{13}$$

127 T_Z is the temperature at depth Z; T is the temperature, q is the heat flux, the subscript T and B denote the top and

128 bottom boundaries of each lithologic layer, respectively; ΔZ is the layer thickness; H is the volumetric heat production; k is

129 the thermal conductivity.

130 We apply a free surface and free slip lower boundary, and impose a 5 cm/yr convergence rate to the trailing end of the

131 procontinental lithosphere. Equivalent material flows out through both side walls of the mantle domain to keep mass balance

132 within the whole computational domain (Fig. 1).
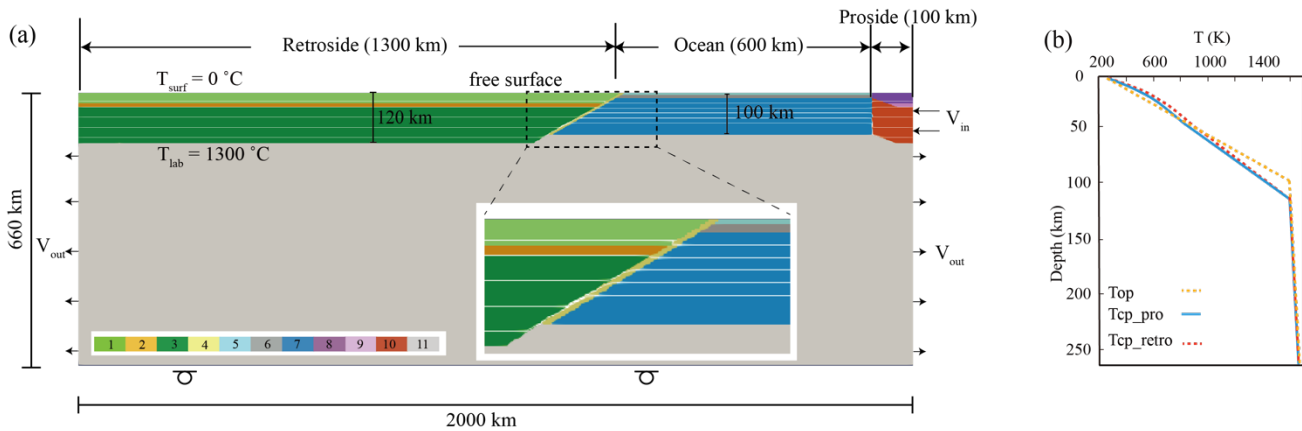
133

134 **Figure 1.** (a) Reference model configuration and boundary conditions. Different colors reflect different lithologies: 1, 8,

135 continental upper crust; 2, 9, continental lower crust; 3, 10, continental lithospheric mantle; 4, weak zone; 5, sediment; 6,

136 oceanic crust; 7, oceanic lithospheric mantle; 11, sub-lithospheric mantle (Table S1). The white lines are isotherms of 200 ˚C

137 increments in the range of 200 ˚C to 1200 ˚C. T_{surf} is the surface temperature, T_{lab} is the bottom temperature of continental

138 lithosphere. V_{in} and V_{out} denote where material flows in and out. (b) Initial distributions of procontinental (T_{cp_pro}),

139 retrocontinental (T_{cp_retro}) and oceanic (T_{op}) lithospheric temperatures.

3 Results

We conducted 48 numerical experiments by varying the moho temperature, upper crustal H_{r_uc} and lower crustal H_{r_lc} of the retrocontinent and procontinent, respectively, to capture different continental thermal structures. Two distinct continental collision evolutionary paths were recognized: (I) continuous subduction and (II) continental subduction with a slab break-off. All the simulations are summarized in Table S2.

3.1 Continuous subduction without slab break-off (Mode I)

Figure 2 shows the development of the continuous subduction mode, and it takes the Model m2 (reference model, Table S2) as an example. The model started with a relative shallow angle subduction characterized by the oceanic plate dips downward along the low-viscosity weak zone (Fig. 2a1, 3 Myr). During this stage, a portion of oceanic sediment was scraped off and stacked at the surface, accompanied by the slight uplift of the retrocontinental foreland (Fig. 2a2, 2c). As the subduction goes on, the dipping angle of the slab in depth gradually steepens due to the increasing slab pull (Fig. 2a2, 9 Myr). At ~11.5 Myr (Fig. 2a3), continents collide with each other after the full consumption of the oceanic plate. Under the continued oceanic slab pulling, the procontinental lithosphere inherited the subduction, characterized by further subducting angle steepening that resulted in the superposition of retrocontinental upper crust and oceanic sediment on the procontinental forepart. With the proceeding of procontinental subduction, the collision wedge uplifted prominently (Fig. 2c). After that, a large part of the oceanic sediment previously scraped off was then entrained and subducted with the procontinental crust, followed by the rapid uplift at the retroside of the collision zone and the retroward advance of suture (Fig. 2c). From ~17.5 Myr on, the buoyant procontinental upper crust began to detach from the underlying lithosphere, mixed with the exhumated oceanic sediment, accumulated together in the subduction channel (Figs. 2a4, 2a5). During this time, uplift within the collision zone gradually expands to the retrocontinental interior (Fig. 2c).
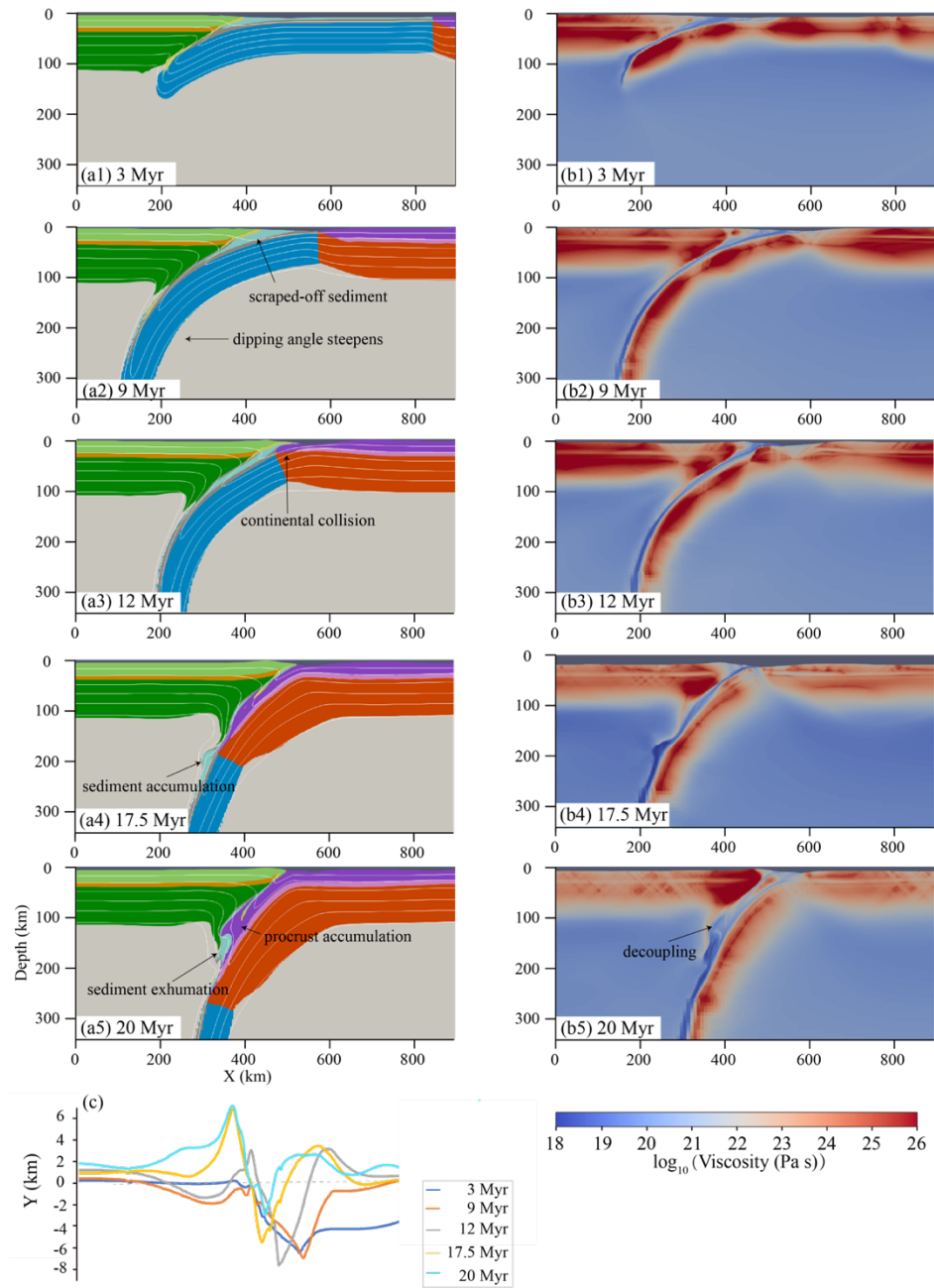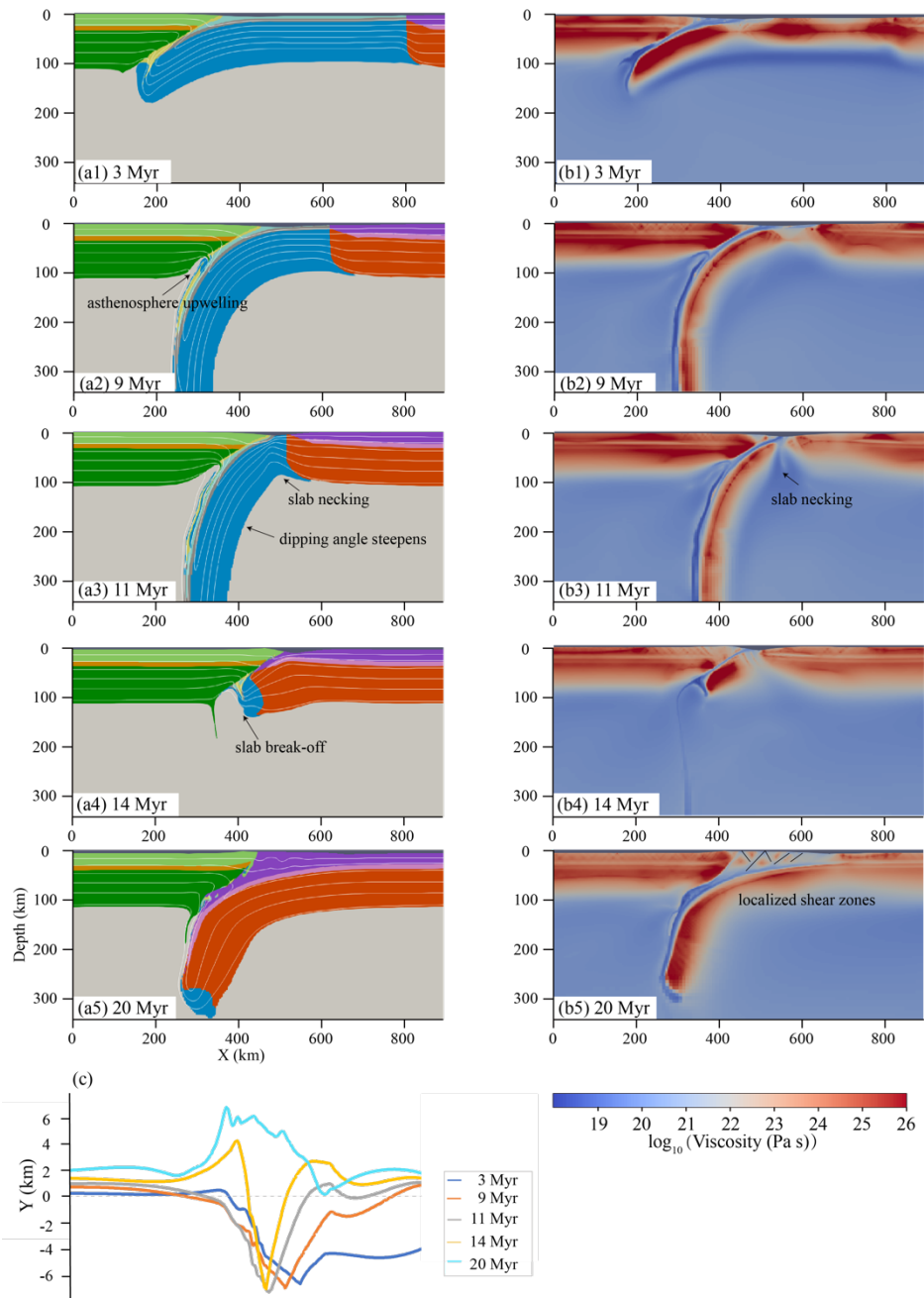
Figure 2. Time evolution of Model m2. Snapshots of compositional fields (a1 - a5), viscosity (b1 - b5) and topography (c) for selected model times are shown. The lithologies and isotherms are the same as in Fig 1.

7

3.2 Continental subduction with a slab break-off (Mode II)

In Model m7, both the pro- and retro- continent have higher T_{moho} than Model m2 (Table S2). The lithospheric deformation behaviors and the evolution of the model during the oceanic subduction phase are quite similar to those observed in Model m2 (Fig. 3a1). The only difference is that the slab steepened more rapidly at a later stage, which gave rise to the decoupling between the retrocontinental lithosphere and the oceanic plate. Such a process created an ideal space for the asthenospheric upwelling and resulted in the significant weakening of the retrocontinental lithosphere (Fig. 3a2, 8.5 Myr). After ~10.2 Myr, combined effect of the increasing slab pull and asthenosphere upwelling promoted necking around the oceanic-procontinental lithospheric transition zone (Fig. 3a3, 11 Myr). The procontinental lithosphere then arrived at the trench and initiated subducting along the inclined weak zone, accommodating most of the ongoing convergence. During this stage, the continuous compression and rebound after slab break-off significantly uplifted the collision zone. Later on, the upper part of the retrocontinental lithosphere indented into the procrust, scraping off most of the procontinental upper crust, causing significant thickening and localized shear zones there while leaving the residual little portion to subduct with the lithosphere. Subsequently, the accumulated orogenic wedge gradually grew into a relatively wide surface uplift.
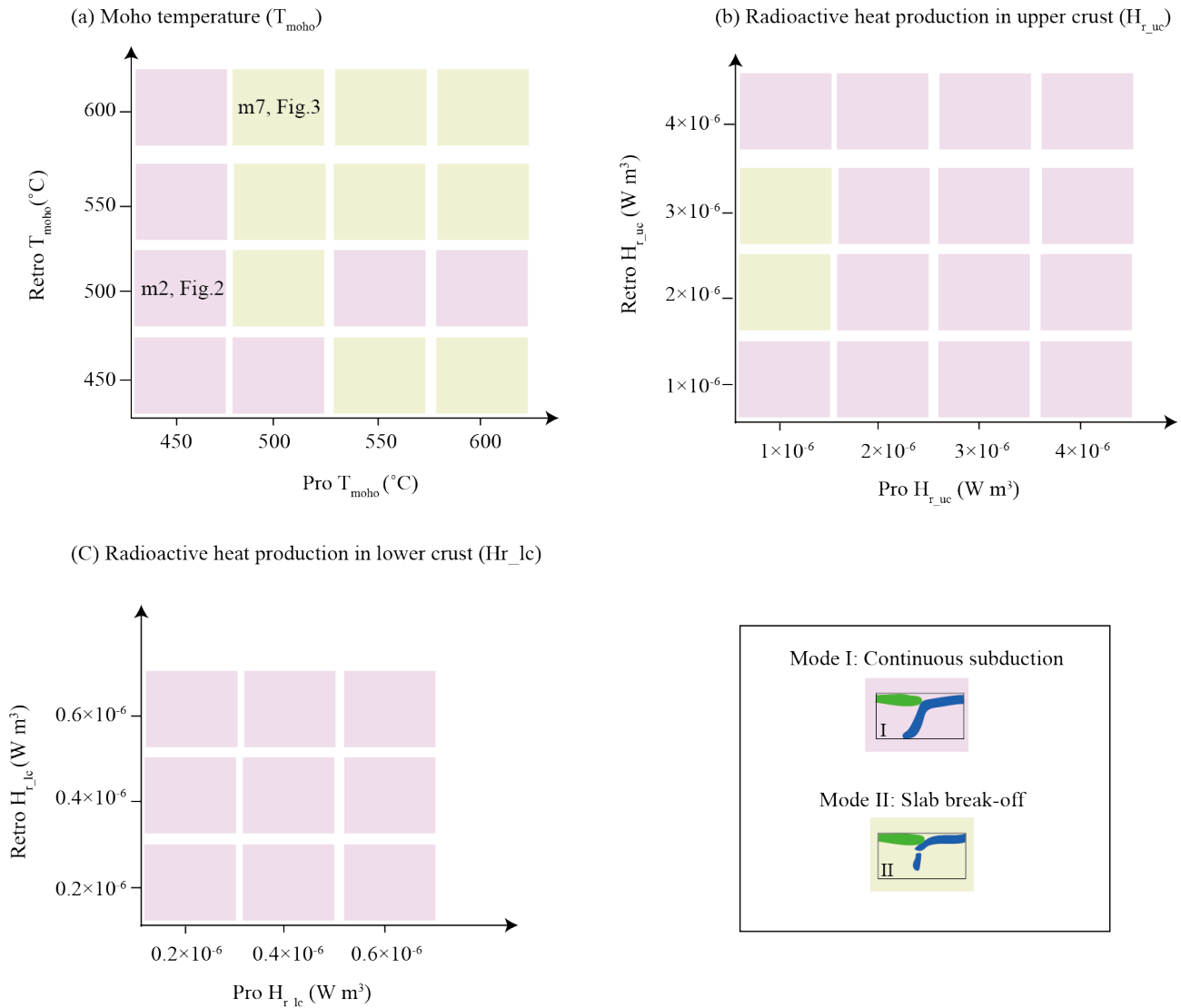
Figure 3. Results of Model m7. Snapshots of compositional fields (a1 - a5), viscosity (b1 - b5) and topography (c) for selected model times are shown. The lithologies and isotherms are the same as in Fig. 1.

3.3 Sensitivity tests of continental lithospheric thermal structure on the evolution of continental convergence

A regime diagram (Fig. 4) of all the models summarizes the template simulations investigating the effects of continental T_{moho} and H_r, and two contrasting end members of continental collision modes are identified. Models with a cold procontinental T_{moho} ($\leq$ 450 °C) generally exhibit a continuous subduction mode without slab break-off. Meanwhile, the hotter the retrocontinental T_{moho}, the steeper the subducting angle is (Figs. 4a, 5a). In comparison, Mode II dominates among the models with a relative hot procontinental T_{moho} ($\geq$ 500 °C), especially when the retrocontinental T_{moho} is greater than 550°C (Fig. 4a). In addition, H_r is a second-order controlling parameter compared to the T_{moho}, as it's more propensity to alter the upper part of lithospheric deformation styles than the continental collision mode (Figs. 6c - 6i).

(a) Moho temperature (T_{moho})

(b) Radioactive heat production in upper crust (H_{r_uc})

(C) Radioactive heat production in lower crust (Hr_lc)

Mode I: Continuous subduction

Mode II: Slab break-off

Figure 4. Schematic figures of models with different (a) continental T_{moho}, (b) upper and (c) lower crustal radioactive heat production (Table S2). The diagram in each panel shows the dependence of collision mode on the corresponding controlling parameters of both colliding plates.

4 Discussions

4.1 How continental moho temperature influences the trajectory of the collision system?

As mentioned above, models incorporating a cold prolithosphere generally evolve into continuous subduction without slab break-off. It may come from the fact that a cold prolithosphere is strong enough to maintain its strength, and also keeps coupling with the retrolithophere during plate convergence. Thus, the prolithosphere suffers moderate roll-back, under the condition that the stress is not sufficient to yield the lithosphere and generate break-off (Fig. 2, Fig. S1 in Supporting Information). Based on further analysis of this mode of models, we notice that the subducting angle increases as the retrocontinental T_{moho} increases, accompanied by much more procrust accumulation at shallow and intense retrolithospheric mantle destruction (Figs. 5a - 5d). The mechanism behind this is that increasing the retrocontinental T_{moho} can weaken the retrolithosphere and increase the thermal structural difference between the two continents, which may lead to plate decoupling. As a consequence, it is more likely for the prolithosphere to roll back as the magnitude of decoupling increases. Besides, weakening of the retrolithosphere may also offer a favorable condition for the intrusion of accumulated procrustal material into it.

As to mode II, models with hot procontinental T_{moho} ($\geq 500°C$) always evolve into continental subduction following a slab break-off. In these models, when the retrocontinental T_{moho} is determined, (1) as the procontinental T_{moho} decreases, the procontinental lithosphere becomes cold, which results in a rheologically strong lithosphere that can be subjected to greater deformation; the slab thus breaks off much latter (Fig. 5e). This is consistent with many of the previous numerical studies (van de Zedde and Wortel, 2001; van Hunen and Allen, 2011; Duretz et al., 2011). However, it appears that Duretz and Gerya (2013) proposed an apparent opposite tendency. It may come from the fact that these models do not use a layered crust. In consequence, a strong crust is more likely to result in strong crust-mantle coupling and a deeper slab break-off under slower convergence, while a weak crust leads to crust-mantle decoupling that may evolve into delamination. (2) The depth of slab break-off in our models is between ~ 30 - 60 km, which is in the range indicated by Davies and von Blanckenburg (1995), Li et al. (2002), Duretz et al. (2011), and Duretz and Gerya (2012). (3) After slab break-off, the buoyant continental lithosphere experiences a rebound accompanied by strong surface uplift within a short duration (Fig. 3c), which coincides with Duretz and Gerya (2013) and Magni et al. (2017). Slab break-off is often considered an early process of continental collision, and numerous numerical simulations have been conducted to investigate it. Comparing their results with our models, we suggest that slab break-off is closely related to the rheological strength of the lithospheres. Therefore, the parameters that have prominent impacts on it, such as oceanic plate age, convergence velocity, continental crustal

structure, layered crustal rheological strength, the strength of the interface between the subducting and overriding plates, etc. (Gerya et al., 2004; Burov, 2011; Duretz et al., 2011; Magni et al., 2017; Koptev et al., 2022), may significantly influence the evolutionary path of slab break-off.

In conclusion, we propose that continental T_{moho} is an important parameter in shaping the continental collision system, especially influencing the fate of subduction. The hotter the procontinent, the weaker and easier it is to evolve into a slab break-off. The hotter either the procontinent or the retrocontinent, the less coupled it is with the adjacent plate. In addition, as a result of ongoing subduction, the slab rolls back rapidly, which may generate a gap between the adjacent plates. The asthenosphere then upwells into it, which in turn aggravates the rollback. This contributes to the development of intense strain localization in the prolithosphere and finally leads to slab break-off (Figs. 3, S2, 5f, 5g, 5h).
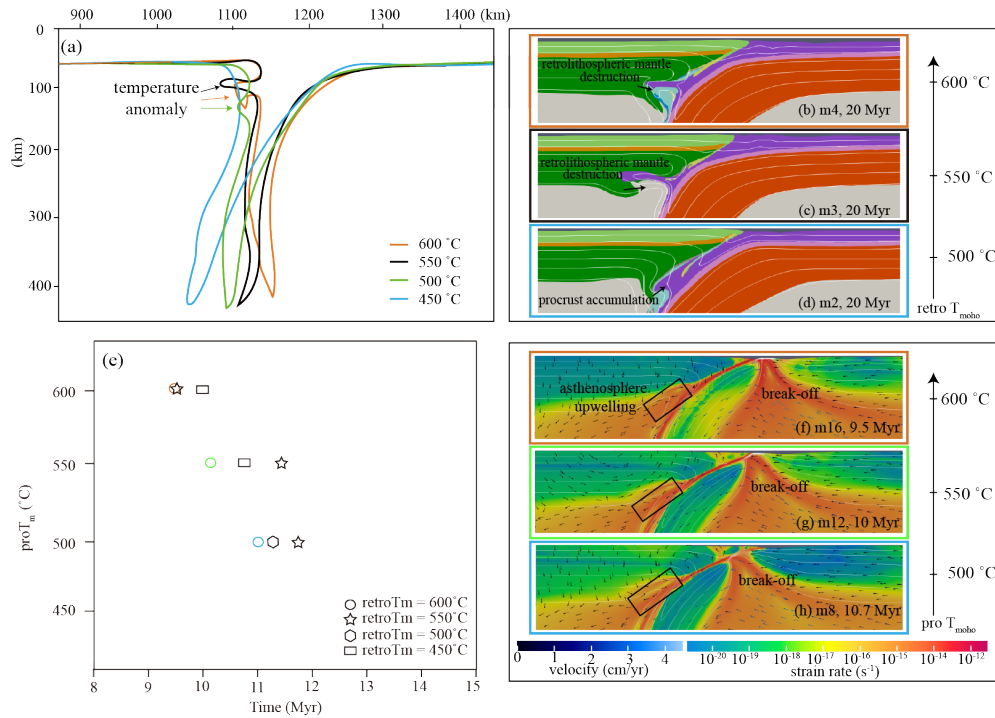

Figure 5. (a) Geometries of subducting plate in models with different retrocontinental T_{moho} outlined by 800 ˚C isotherms. Compositional fields of models with decreasing retrocontinental T_{moho}, (b) m4, retro T_{moho} = 600°C, (c) m12, retro T_{moho} = 550°C, (d) m8, retro T_{moho} = 500°C. White lines denote the isotherms (200 ˚C increments). (e) shows the relationship between the times of slab break-off and continental T_{moho}. (f)-(h) are strain rate of models with various procontinental T_{moho}.

4.2 How crustal radioactive heat production influences the trajectory of the collision system

Radioactive elements are thought to mainly exist in the continental crust, and the radioactive heat production that originates from their decay is one of the important internal heat sources in the earth, which influences the continental

237 lithospheric thermal structure significantly (Turcotte and Schubert, 2002; Faccenda et al., 2008). According to our model

238 results, increasing the upper crustal H_r can distinctly increase the thermal gradient of the lithospheric upper part, under the

239 effect of which the steep surface topography built at the early stage of continental collision would tend to be relatively gentle.

240 In comparison, varying lower crustal H_r has much less influence on the variation of the continental lithospheric thermal

241 gradient and the evolution of surface topography. Moreover, as the H_r in the crust increases, the lithospheric rheological

242 strength decreases, which facilitates the growth of crustal shear zones. That is, the higher the crustal H_r, the more shear zones

243 it may generate in the crust (Figs. 6c - 6i). In conclusion, crustal H_r is a crucial parameter in enhancing strain localization in

244 the lithospheric upper part that is closely related to the growth of shear zones, while it exerts a second-order influence on

245 altering the continental collision mode.
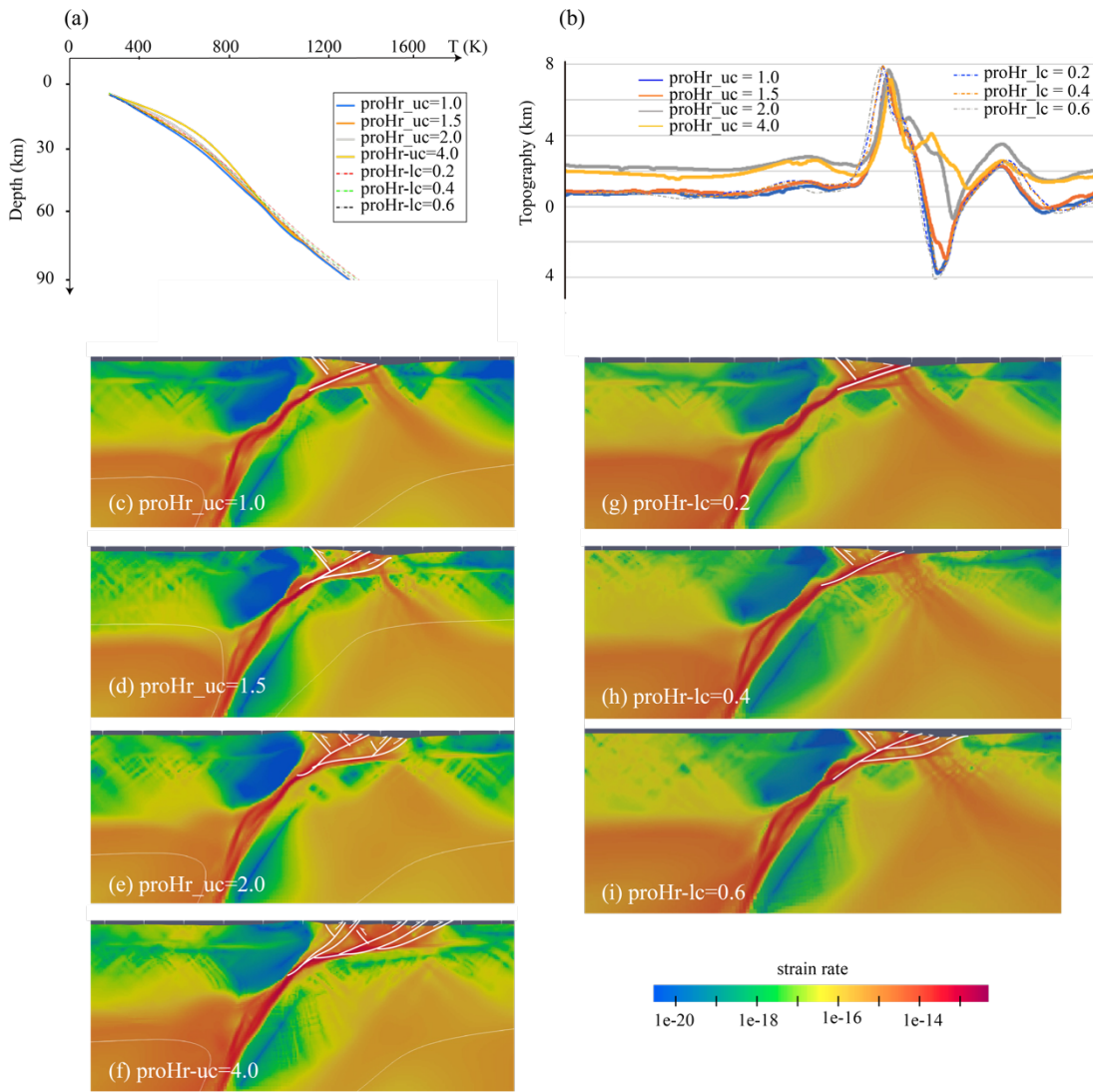
246

247　**Figure 6**. Temperature profiles (a), topography (b) and strain rate (c-i, at 20 Myr) of models with different crustal H_r.

248

249　**4.3 Implications for the development of lateral heterogeneity of Indian-Asian collision**

250　　　　~2000 km-long east-west Himalayan-Tibetan orogenic system was created by continental collision from ~ 60 to 50

251　Ma, with the Nanga Parbat syntaxis as its west margin and the Namche Barwa syntaxis in the east (Chen et al., 2015). It has

252　been proven by contrasting along-strike lithospheric structures (Li et al., 2008; Chen et al., 2015; Kufner et al., 2021). By

253　comparison, our models are capable of providing several first-order fits of the crust-mantle deformation behaviors to this

254　natural collision system, especially at the Hindu-Kush profile and the eastern Tibet profile.

255　　　　Hindu Kush is the westernmost end of the Himalayan-Tibetan orogen. Previous seismic tomography studies have

256　confirmed that there is a north-dipping, downward steepening, and thinning high-velocity anomaly (HVA), accompanied by

257　increasingly intense seismicity, underneath the region (Kufner et al., 2016; Kufner et al., 2021). The inclined HVA is

258　believed to be a subducting plate of Indian provenance and is part of the Indian-Asian collision system. The thinning of the

259　HVA is in the extent between 180-220 km, and was suggested to be at the transition zone between Indian continental

260　lithosphere and Neo-Tethys oceanic lithosphere. In agreement with the observations, Model m2 has a similar tectonic

261　background, and shows an analogous continuous subduction characterized by a nearly vertical dipping angle and a slab

262　necking at a depth of ~ 220 km. In addition, the relative narrow collision orogen in the model is also consistent with the

263　natural topography in this region (Figs. 7a, 2c). It's worth noticing that the observed inclined distribution of earthquakes

264　seems to coincide with the subducting continental crust. This may offer a possible explanation for the active intermediate

265　earthquakes beneath this region.

266　　　　The main part of the Himalayan-Tibetan orogen is the product of a collision between the cold Indian craton and the

267　relative warm Asian continent after the closure of Neo-Tethys, the geological settings of which are quite analogous with our

268　Model m7. During the continental collision phase, the Yarlung Zangbo suture zone bordering the Indian and Asian

269　lithospheres moved significantly, creating an～8 km mountain (the Himalayas) and a ~ 4 km plateau (the Tibetan Plateau)

270　(Yin and Harrison, 2000). Unlike continuous subduction underlying the Hindu Kush, geological and seismological evidence

271　shows that the eastern part of the profile is underlain by a shallower-angle subducting Indian lithosphere following a slab

272　break-off; these are also similar to the model results of Model m7 (Figs. 7b, 2c). Furthermore, previous field observations

273　have shown that the northern part of the Indian continental crust is abundant with radioactive elements (Vidal et al., 1982;

274　Scaillet et al., 1990; Macfarlane, 1992; Faccenda et al., 2008). Our sensitive tests have recognized that continental crust with

275　high radioactive heat production is much easier to generate brittle fractures and intense deformation of the lithospheric upper

276　part, which may lead to the development of new shear zones (Fig. 6). This resembles the tectonic characteristics of large

277　thrust fault zones in the Himalayas (Fig. 7b).

278　　　　In consequence, we speculate that the continental lithospheric thermal structural difference may be one of the key

279　parameters that control the evolution of lateral heterogeneity along the Himalayan-Tibetan orogen and that the high content

14

280   of crustal radioactive elements is one of the significant factors that dominates the growth of large thrust fault zones in the

281   Himalayas.
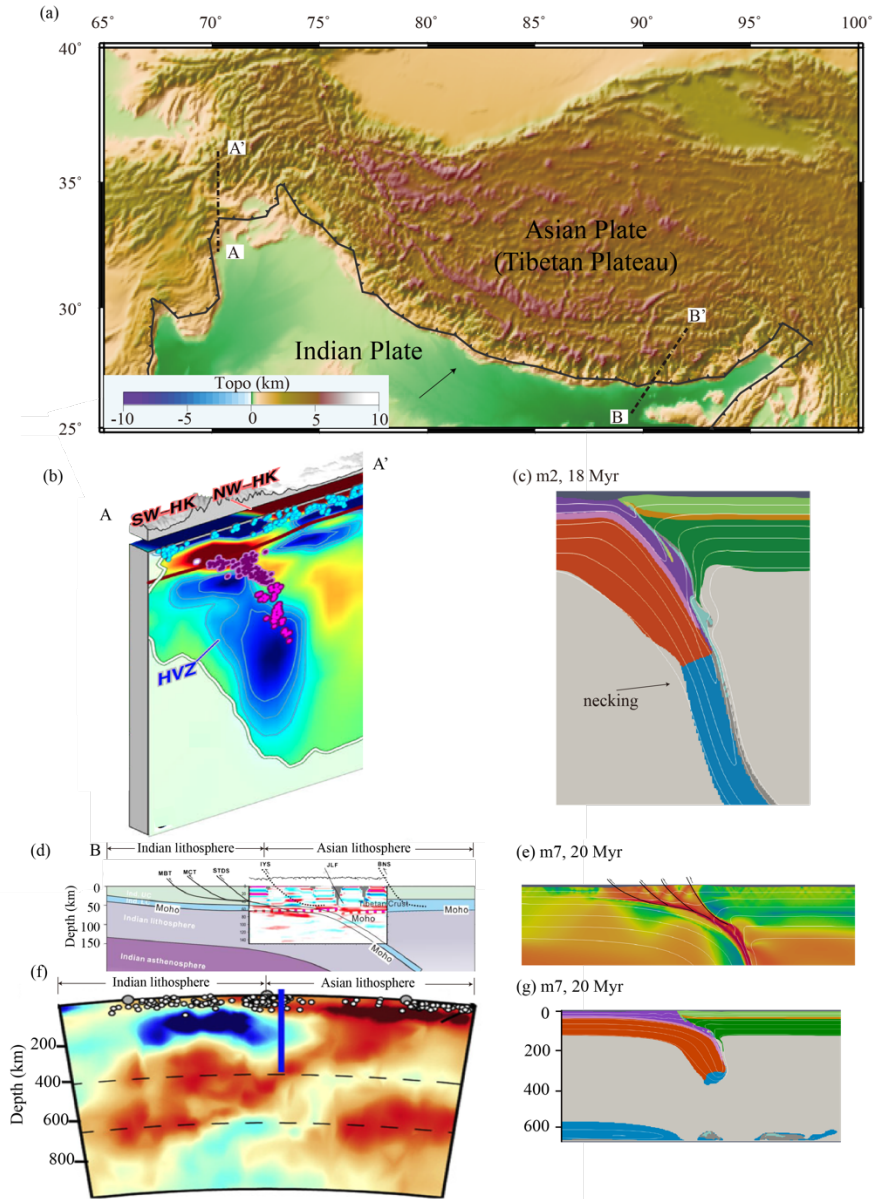
282

283   **Figure 7.** (a) Geographic setting of Himalayan-Tibetan orogen. Schematic geologic cross-sections across the (b) western

284   (Hindu Kush) (Kufner et al., 2021) and eastern Himalayan-Tibetan orogen (Li et al., 2008; Wang et al., 2019). (c) shows the

285   compositional field of Model m2 (mode I), (e) and (g) are the strain rate and compositional field of Model m7 (mode II),

286   respectively.

287

5 Conclusions

In this work, we systematically discuss the influences of the continental lithospheric thermal structure on the evolution of the continental collision system based on high-resolution thermomechanical numerical experiments. The model results demonstrate that:

Two end members of continental collision are obtained: the continuous subduction mainly occurs with a relative cold overriding lithosphere ($T_{moho} \leq 450°$), and as the retrocontinental T_{moho} increases, the subducting angle steepens. Slab break-off dominates when the model has a relatively hot procontinental T_{moho} (≥ 500 °C), especially when the retrocontinental T_{moho} is greater than 550°C. H_r is a second-order controlling parameter compared with T_{moho} in shaping the continental collision mode, while it is more prone to facilitate the growth of crustal shear zones.

The continental lithospheric thermal structure may have played a significant role in the development of lateral heterogeneity along the Himalayan-Tibetan orogenic belt. We suggest that the different evolutionary paths between the continuous subduction underlying the Hindu Kush and the continental subduction beneath eastern Tibet may come from the inherited lateral variation of the Indian lithospheric geothermal gradient. In addition, the high content of radioactive elements in the continental crust may be one of the important reasons for the development of deep and large thrust fault zones in this collision orogen.

Competing interests. The authors declare that they have no conflict of interest.

Author contributions. MXL and DHY designed and oversaw the project. MXL performed all the numerical simulations. R.Q. participated in the discussions and paper revisions. All authors contributed to the manuscript writing.

References

Arndt, D., Bangerth, W., Blais, B., Fehling, M., Gassmöller, R., Heister, T., Heltai, L., Köcher, U., Kronbichler, M., Maier, M., Munch, P., Pelteret, J.-P., Proell, S., Simon, K., Turcksin, B., Wells, D., and Zhang, J.: The deal.II library, Version 9.3. J. Numer. Math., 29 (3), 171-186, https://doi.org/10.1515/jnma-2021-0081, 2021.

Beaumont, C., Fullsack, P., and Hamilton, J.: Styles of crustal deformation in compressional orogens caused by subduction of the underlying lithosphere. Tectonophysics, 232, 119-132, https://doi.org/10.1016/0040-1951(94)90079-5, 1994.

Burov, E. B.: Rheology and strength of the lithosphere. Marine and Petroleum Geology, 28(8): 1402-1443, https://doi.org/10.1016/j.marpetgeo.2011.05.008, 2011.

Chapman, D. S.: Thermal gradients in the continental crust. Geological Society, London, Special Publications 24, 63-70, https://doi.org/10.1144/GSL.SP.1986.024.01.0, 1986.

Chen, L., and Gerya, T. V.: The role of lateral lithospheric strength heterogeneities in orogenic plateau growth: Insights from 3-D thermo-mechanical modeling, J. geophys. Res.: Solid Earth, 121(4), 3118-3138, https://doi.org/10.1002/2016JB012872, 2016.

Chen, Y., L, W., Yuan, X. H., Badal, J., and Teng, J. W.: Tearing of the Indian lithospheric slab beneath southern Tibet revealed by SKS-wave splitting measurements. Earth Planet. Sci. Lett., 413: 13-24, https://doi.org/10.1016/j.epsl.2014.12.041, 2015.

Davis, R.O., and Selvadurai, A.P.S.: Plasticity and Geomechanics. Cambridge University Press, Cambridge, 2002.

Davies, H. J., and F. von Blanckenburg.: Slab breakoff: A model of lithosphere detachment and its test in the magmatism and deformation of collisional orogens. Earth Planet. Sci. Lett., 129(1): 85-102, https://doi.org/10.1016/0012-821X(94)00237-S, 1995.

Duretz, T. and Gerya, T. V.: Slab detachment during continental collision: Influence of crustal rheology and interaction with lithospheric delamination. Tectonophysics, 602: 124-140, https://doi.org/10.1016/j.tecto.2012.12.024, 2013.

Duretz, T., Gerya, T. V., and D. A. May.: Numerical modelling of spontaneous slab breakoff and subsequent topographic response. Tectonophysics, 502(1): 244-256, https://doi.org/10.1016/j.tecto.2010.05.024, 2011.

Duretz, T., Schmalholz, S. M., and Gerya, T. V.: Dynamics of slab detachment. Geochem, Geophy, Geosy, 13(3), https://doi.org/10.1029/2011GC004024, 2012.

Faccenda, M., Gerya, T.V., and Chakraborty, S.: Styles of post-subduction collisional orogeny: Influence of convergence velocity, crustal rheology and radiogenic heat production. Lithos, 103, 257-287, https://doi.org/10.1016/j.lithos.2007.09.009, 2008.

Ghazian, R.K., and Buiter, S.J.H.: A numerical investigation of continental collision styles. Geophys. J. Int., 193, 1133-1152, https://doi.org/10.1093/gji/ggt068, 2013.

Gerya, T. V., Yuen, D. A., and Maresch, W. V.: Thermomechanical modelling of slab detachment. Earth Planet. Sci. Lett., 226(1): 101-116, https://doi.org/10.1016/j.epsl.2004.07.022, 2004.

353 Gleason, G.C., and Tullis, J.: A flow law for dislocation creep of quartz aggregates determined with the molten salt cell.
354　　Tectonophysics 247, 1-23, https://doi.org/10.1016/0040-1951(95)00011-B, 1995.

355 Glerum, A., Thieulot, C., Fraters, M., Blom, C., and Spakman, W.: Nonlinear viscoplasticity in ASPECT: benchmarking and
356　　applications to subduction. Solid Earth, 9, 267-294, https://doi.org/10.5194/se-9-267-2018, 2018.

357 Heron, P.J., and Pysklywec, R.N.: Inherited structure and coupled crust-mantle lithosphere evolution: Numerical models of
358　　Central Australia. Geophys. Res. Lett., 43, 4962-4970, https://doi.org/10.1002/2016GL068562, 2016.

359 Hirth, G., and Kohlstedt, D.: Rheology of the upper mantle and the mantle wedge: A view from the experimentalists.
360　　Washington DC American Geophysical Union Geophysical Monograph Series, 138, 83-105,
361　　https://doi.org/10.1029/138GM06, 2003.

362 Huangfu, P., Li, Z.H., Fan, W., and Shi, Y.: Dynamics of crustal overthrust versus underthrust in the continental collision
363　　zones: Numerical modelling. Terra Nova, 31, 332-342, https://doi.org/10.1111/ter.12384, 2019.

364 Huangfu, P., Wang, Y., Fan, W., Li, Z., and Zhou, Y.: Dynamics of unstable continental subduction: Insights from numerical
365　　modeling. Sci. China. Earth. Sci., 60, 218-234, https://doi.org/10.1007/s11430-016-5014-6, 2017.

366 Karato, S.-i., and Wu, P.: Rheology of the upper mantle: A synthesis. Science, 260, 771-778,
367　　https://doi.org/10.1126/science.260.5109.771, 1993.

368 Karato, S.-i.: Deformation of Earth Materials: An Introduction to the Rheology of Solid Earth. Cambridge University Press,
369　　Cambridge, 2008.

370 Koptev, A., Ehlers, T. A., Nettesheim, M., and Whipp, D. M.: Response of a Rheologically stratified lithosphere to
371　　subduction of an indenter-shaped plate: Insights into localized exhumation at orogen syntaxes. Tectonics, 38(6): 1908-
372　　1930, https://doi.org/10.1029/2018TC005455, 2019.

373 Koptev, A., Nettesheim, M. and Ehlers, T. A.: Plate corner subduction and rapid localized exhumation: Insights from 3D
374　　coupled geodynamic and geomorphological modelling. Terra Nova, 34(3): 210-223, https://doi.org/10.1111/ter.12581,
375　　2022.

376 Kronbichler, M., Heister, T., and Bangerth, W.: High accuracy mantle convection simulation through modern numerical
377　　methods. Geophys. J. Int., 191, 12-29, https://doi.org/10.1111/j.1365-246X.2012.05609.x, 2012.

378 Kufner, S. K., Kakar, N., Bezada, M., Bloch, W., and Schurr, B.: The Hindu Kush slab break-off as revealed by deep
379　　structure and crustal deformation. Nature Communications, 12: 1685, https://doi.org/10.1038/s41467-021-21760-w,
380　　2021.

381 Kufner S. K., Schurr, B., Sippl, C., Yuan, X. H., Ratschbacher, L., Akbar, A. M., Ischuk, A., Murodkulov, S., Schneider, F.,
382　　Mechie, J., and Tilmann, F.: Deep india meets deep asia: lithospheric indentation, delamination and break-off under
383　　pamir and hindu kush (central asia). Earth Planet. Sci. Lett., 435, 171-184, https://doi.org/10.1016/j.epsl.2015.11.046,
384　　2016.

385 Li, C., van der Hilst, R. D., Meltzer, A. S., and Engdahl, E. R.: Subduction of the Indian lithosphere beneath the Tibetan
386　　Plateau and Burma. Earth Planet. Sci. Lett. 274, 157–168, https://doi.org/10.1016/j.epsl.2008.07.016, 2008.

387   Li, L., Liao, X., and Fu, R.: Slab breakoff depth: A slowdown subduction model. Geophys. Res. Lett., 29(3): 11-11-11-13,
388   https://doi.org/10.1029/2001GL013420, 2002.

389   Liao, J., and Gerya, T.: Partitioning of crustal shortening during continental collision: 2-D thermomechanical modeling. J.
390   geophys. Res., 122, 592-606, https://doi.org/10.1002/2016JB013398, 2017.

391   Liu, M., and Yang, D. H.: How do pre-existing weak zones and rheological layering of the continental lithosphere influence
392   the development and evolution of intra-continental subduction? J. Asian. Earth. Sci., 238, 105385,
393   https://doi.org/10.1016/j.jseaes.2022.105385, 2022.

394   Liu, M., Yang, D. H., and Huangfu, P. P.: Effects of plate velocity slowdown on altering continental collision patterns and
395   crustal-lithospheric deformation during the collision process. Front. Earth Sci., 10: 814710,
396   https://doi.org/10.3389/feart.2022.814710, 2022a.

397   Liu, S., Sobolev, S.V., Babeyko, A.Y., and Pons, M.: Controls of the foreland formation pattern in the orogen-foreland
398   shortening system: constraints from high-resolution geodynamic models. Tectonics, 41, e2021TC007121,
399   https://doi.org/10.1029/2021TC007121, 2022b.

400   Luth, S., Willingshofer, E., Sokoutis, D., and Cloetingh, S.: Analogue modelling of continental collision: Influence of plate
401   coupling on mantle lithosphere subduction, crustal deformation and surface topography. Tectonophysics, 484, 87-102,
402   https://doi.org/10.1016/j.tecto.2009.08.043, 2010.

403   Macfarlane, A.M.: The tectonic evolution of the core of the Himalaya, Langtang National Park, central Nepal. Massachusetts
404   Institute of Technology, 1992.

405   Magni, V., Allen, M. B., van Hunen, J., and Bouilhol, P.: Continental underplating after slab break-off. Earth Planet. Sci.
406   Lett., 474: 59-67, https://doi.org/10.1016/j.epsl.2017.06.017, 2017.

407   Nettesheim, M., Ehlers, T. A., Whipp, D. M., and A. Koptev, A.: The influence of upper-plate advance and erosion on
408   overriding plate deformation in orogen syntaxes. Solid Earth 9(6): 1207-1224, https://doi.org/10.5194/se-9-1207-2018,
409   2018.

410   Pysklywec, R.N.: Evolution of subducting mantle lithosphere at a continental plate boundary. Geophys. Res. Lett., 28, 4399-
411   4402, https://doi.org/10.1029/2001GL013567, 2001.

412   Rybacki, E., Gottschalk, M., Wirth, R., and Dresen, G.: Influence of water fugacity and activation volume on the flow
413   properties of fine-grained anorthite aggregates. J. geophys. Res., 111, B03203, https://doi.org/10.1029/2005JB003663,
414   2006.

415   Scaillet, B., France-Lanord, C., and Le Fort, P.: Badrinath-Gangotri plutons (Garhwal, India): petrological and geochemical
416   evidence for fractionation processes in a high Himalayan leucogranite. J. Volcanol. Geoth. Res., 44, 163-188,
417   https://doi.org/10.1016/0377-0273(90)90017-A, 1990.

418   Tang, J., Chen, L., Meng, Q., and Wu, G.: The effects of the thermal state of overriding continental plate on subduction
419   dynamics: Two-dimensional thermal-mechanical modeling. Sci. China. Earth., Sci, 63, 1519-1539,
420   https://doi.org/10.1007/s11430-019-9624-1, 2020.

421 Toussaint, G., Burov, E., and Jolivet, L.: Continental plate collision: Unstable vs. stable slab dynamics. Geology, 32, 33-36,
422   https://doi.org/10.1130/G19883.1, 2004.

423 Turcotte, D.L., and Schubert, G.: Geodynamics. Cambridge university press. 2002

424 Ueda, K., Gerya, T.V., and Burg, J.-P.: Delamination in collisional orogens: Thermomechanical modeling. J. geophys. Res.,
425   117, B08202, https://doi.org/10.1029/2012JB009144, 2012.

426 van Zelst, I., F. Crameri, A. E. Pusok, A. Glerum, J. Dannberg, and C. Thieulot.: 101 geodynamic modelling: how to design,
427   interpret, and communicate numerical studies of the solid Earth. Solid Earth, 13(3), 583-637, https://doi.org/10.5194/se-
428   13-583-2022, 2022.

429 van Hunen, J. and Allen, M. B.: Continental collision and slab break-off: A comparison of 3-D numerical models with
430   observations. Earth Planet. Sci. Lett., 302(1): 27-37, https://doi.org/10.1016/j.epsl.2010.11.035, 2011.

431 Vidal, P., Cocherie, A., and Fort, P.L.: Geochemical investigations of the origin of the Manaslu leucogranite (Himalaya,
432   Nepal). Geochim. Cosmochim. Ac., 46, 2279-2292, https://doi.org/10.1016/0016-7037(82)90201-0, 1982.

433 Vogt, K., Willingshofer, E., Matenco, L., Sokoutis, D., Gerya, T., and Cloetingh, S.: The role of lateral strength contrasts in
434   orogenesis: A 2D numerical study. Tectonophysics, 746, 549-561, https://doi.org/10.1016/j.tecto.2017.08.010, 2018.

435 Wang, C. Y., Mooney, W. D., Zhu, L., Wang, X., Lou, H., and You, H., Cao, Z., Chang, L., and Yao, Z.: Deep structure of
436   the eastern himalayan collision zone: evidence for underthrusting and delamination in the postcollisional stage.
437   Tectonics, 38,3614-3628, https://doi.org/10.1029/2019TC005483, 2019.

438 Wessel, P., Smith, W.H.F., Scharroo, R., Luis, J., and Wobbe, F.: Generic Mapping Tools: Improved Version Released. Eos,
439   Transactions American Geophysical Union, 94, 409-410, https://doi.org/10.1002/2013EO450001, 2013.

440 Wilks, K.R., and Carter, N.L.: Rheology of some continental lower crustal rocks. Tectonophysics, 182, 57-77,
441   https://doi.org/10.1016/0040-1951(90)90342-6, 1990.

442 Willingshofer, E., and Sokoutis, D.: Decoupling along plate boundaries: Key variable controlling the mode of deformation
443   and the geometry of collisional mountain belts. Geology, 37, 39-42, https://doi.org/10.1130/G25321A.1, 2009.

444 Yin, A., and Harrison, T.M.: Geologic Evolution of the Himalayan–Tibetan Orogen. Annu. Rev. Earth. Pl. Sc., 28, 211-280,
445   2000

446 Zhou, H. W., and Murphy, M. A.: Tomographic evidence for wholesale underthrusting of india beneath the entire tibetan
447   plateau. J. Asian. Earth. Sci., 25(3), 445-457, https://doi.org/10.1016/j.jseaes.2004.04.007, 2005.